Pd–H and Ni–H phase diagrams using cluster variation method and Monte Carlo simulation

Natacha Bourgeois, Pierre Cenedese, Jean-Claude Crivello, Jean-Marc Joubert

PHILOSOPHICAL MAGAZINE

Pd–H and Ni–H Phase Diagrams using Cluster Variation Method and Monte-Carlo Simulation

Natacha Bourgeois[a], Pierre Cenedese[a], Jean-Claude Crivello[a] and Jean-Marc Joubert[a]

[a]Université Paris Est, ICMPE (UMR 7182), CNRS, UPEC, F-94320 Thiais, France

ARTICLE HISTORY

Compiled March 27, 2019

ABSTRACT

This work focuses on interstitial solid solutions of hydrogen in the face centered cubic (fcc) host lattice of palladium and nickel, using a first-principles based approach. Cluster Variation Method (CVM) and Monte Carlo simulation algorithms were especially designed, allowing a coupled use of both techniques, to study hydrogen-vacancy interactions inside a fcc metallic host lattice. First-principles calculations provided the H–Vac interaction energies by structure inversion method. The phase diagrams and thermodynamic properties were computed using only theoretical inputs. The mechanisms leading to the formation of the miscibility gaps observed for both Pd–H and Ni–H systems and the hydrogen ordering on palladium interstitial lattice were reproduced without any empirical term.

PACS CLASSIFICATION

63.20.dk 88.30.R- 88.30.rd 88.30.G- 65.40.gd 07.05.Tp 61.43.Bn 64.75.Nx

KEYWORDS

Metal hydrides; Computer modelling and simulation; miscibility gap.

CONTACT Jean-Claude Crivello. Email: crivello@icmpe.cnrs.fr

1. Introduction

Among metal-hydrogen systems, Pd–H and Ni–H have been of particular interest from both fundamental and application points of view. Palladium and nickel are involved in many hydrogen technologies such as hydrogen storage alloys [1, 2], hydrogen detection [3], purification [4], isotope separation and storage or electrode for nickel-metal-hydride batteries [5, 6].

Pd and Ni are isoelectronic and the phase diagrams of Pd–H and Ni–H systems are similar: it consists in an interstitial solid solution of hydrogen occupying the octahedral (O) sites of the face centered cubic (fcc) metallic lattice. This has been shown both experimentally [7, 8] and theoretically [9]. A miscibility gap is present in both systems, observable at atmospheric pressure in Pd–H and above 340 MPa in Ni–H. It corresponds to the two-phase equilibrium between hydrogen poor α and rich α' phases with the same fcc structure.

Despite these similarities, a specificity of the Pd–H system is the short-range ordering of hydrogen atoms and vacancies on the O-sites [10, 11] and the presence of two super-structures ($PdH_{0.5}$ and $PdH_{0.8}$) observed by neutron diffraction at low temperature [12–16] (Table 1). The two experimentally observed hydrides can be described by successions of (420) planes: two hydrogen filled + two vacant at H/M=y(H)=0.5 ($I4_1/amd$) and four hydrogen filled + one vacant at y(H)=0.8 ($I4/m$). At a first glance, these features seem to be incompatible with the presence of a miscibility gap.

Table 1. Observed super-structures for the Pd–H system at low temperature. Composition, Pearson Symbol (P.S.) , Space Group (S.G.) (number), Wyckoff positions.

H/M	P.S.	S.G. (number)	Wyckoff position
0.5	$tI12$	$I4_1/amd$ (141)	M: 8e, H : 4a
0.8	$tI10$	$I4/m$ (87)	M: 8h, 2a, H : 8h

The wide interest in the Pd–H system motivated modelling attempts since the 1930s. Before the discovery of the low temperature ordering, the first phenomenological model of Lacher [17], later developed by Harasima *et al.* [18], accounted only for the phase separation, supposing a constant attractive H–H first neighbour pair interaction. This attractive interaction reflects the segregation of hydrogen atoms which corresponds at the macroscopic scale to the phase separation. Later on,

Brodowski [19] introduced 2 independent energetic contributions: (1) an electronic contribution arising from the chemical bonds between atoms on a rigid lattice and (2) a contribution arising from the lattice expansion around interstitialhydrogen atoms, leading to an indirect attractive interaction between hydrogen atoms, responsible for the phase separation. Weaknesses of these approaches have been pointed out by Oates [20] as the oversimplified hypothesis of independent protonic and electronic energetic contributions.

In contrast to the theory of Cahn [21], in the concept developed by Alefeld [22, 23], the long range elastic interaction arising from the lattice expansion with the α' phase growth are supposed to favour the phase separation in M–H systems. The corresponding energetic contribution depends only on H-composition and can be regarded as indirect H–H attractive interactions.

Bond and Ross [24] proposed the first Monte Carlo (MC) simulation accounting for the ordering tendency, expressed, this time, by a repulsive H–H first neighbour interaction. Based on Alefeld's work, they considered the phase separation as arising from a configuration independent long-range contribution which was not included in the simulation. The energies associated with the H–H first and second neighbour pair interactions were especially chosen in order to stabilize one of the experimentally observed super-structures.

Picton *et al.* [25] extended Bond and Ross approach introducing long-range interactions in MC simulation to include, in a rough approach, the miscibility gap. Thereafter, Mohri and Oates [26, 27] used the Cluster Variation Method (CVM) to design a comprehensive description of Pd–H. The atomic interaction energies reflect the ordering tendency, while the phase separation is promoted by a configuration independent energy contribution, representing the effect of the lattice expansion. A subsequent CVM model [28] returned however to an attractive H–H first neighbour interaction to describe only the miscibility gap in palladium-based alloys. In addition to these studies, the semi-empirical Calphad model of Joubert and Thiébaut [29] describes the behaviour of Pd–H system based on experimental data above room temperature with repulsive H–H interactions (attractive H–Vac interactions but neglects the low temperature ordering.

In comparison with Pd–H, the experimental data on Ni–H system are scarce. The thermodynamic modeling Calphad method [30, 31] was only recently employed to describe the thermodynamic behavior of the system, gathering all the available experimental data and adding theoretical results from the Cluster Expansion Method (CEM) [32].

The objective of the present study was to propose the first model of the Ni–H and Pd–H systems using statistical thermodynamics without any empirical parameter and to clarify the similarities and differences between the two systems. Considering the metal host lattice as fixed, the cluster energies of the H–Vacancy sub-system on the O-sites, were determined using various approaches. For this purpose, we used Density Functional Theory (DFT) calculations of ordered structures generated in the frame of the CEM. They were used as input data for the CVM and MC simulations and to determine a comprehensive picture of the configurational dependence of the solid solution energy. The two similar systems Ni–H, and Pd–H were thus jointly treated using the same methods combining the input data of the DFT with CVM and MC simulation, via the CEM as an interface.

2. Methodologies

2.1. CVM

The configurational entropy is approximated within the variational approach developed by Kikuchi [33] applied to the pseudo-binary system hydrogen–vacancy occupying the fcc octahedral interstitial sublattice of the fcc host lattice.
In the following, we considered mainly the 13-14 points clusters, and in the case of Ni–H the isotropic rhombohedral was also used as basic cluster. These two approximations are known to give fairly accurate results. The anisotropic rhombohedral cluster approximation which was considered by Pelizzola [34] leads exactly to the same results.

The minimization was carried out not only using the correlation function formalism [35] (case 1) but also in a pure probability framework (case 2). Each approach

has its own advantages, allowing to design several minimization algorithms. We now recall the main steps needed in the two CVM contexts.

Within the two formalisms, for a given basic cluster approximation (13-14 or rhombohedral), the first step is to define the independent cluster probabilities of configurations from space group symmetry operations. Unless the basic clusters were simplex, as for example tetrahedron or octahedron, lattice translations define either cuts leading to correlation functions, the independent variables, or to equality constraints among probabilities. For example, writing the probabilities of finding an A or B atoms (equivalently spin up or down in the Ising model), is defined as $p_{\pm} = \frac{1 \pm \xi_1}{2}$ where $\xi_{\emptyset} = 1$ stands for the free ensemble and ξ_1 the point correlation function. The whole set of linear equations and the matrix M in Eq. 2 linking the probabilities to the correlation functions, including those of sub-clusters, are thus obtained from Kronecker products of the two by two matrix in case of $M(1,1) = \frac{1}{2}\begin{pmatrix} 1 & 1 \\ 1 & -1 \end{pmatrix}$, associated to pure mean field involving free ensemble and point correlation. It is followed by appropriate rows and columns concatenation or by defining sub-cluster probabilities as symmetrized positive linear combination of basic cluster ones in probability formalism. It should be stated here that both approaches lead to exactly the same outcome.
Following the above procedures, the grand-potential $\beta\, G = \beta\, F - \beta\mu\, \xi_1$, with μ the effective chemical potential and ξ_1 the point correlation function, can be written in standard form.
In case 1, we have :

$$\beta\, G = \sum_{i=1}^{n_c} \beta\, \nu_i\, \xi_i - \beta\, \mu\, \xi_1 + \sum_{j=1}^{n_p} a_j\, p(j)\, \big(\ln p(j) - 1\big) \tag{1}$$

$$p(j) = \sum_{i=1}^{n_c} M\,(j,i)\; \xi_i \geq 0 \tag{2}$$

where the subscripts i and j label the correlation functions and the probabilities, respectively, and array ξ_i accounts for the n_c correlation functions including the empty ensemble $\xi_0 = 1$, $p(j)$ for $j \in [1, n_p]$ accounts for the n_p probabilities including those

of sub-clusters. Finally, array ν_i stands for the Effective Cluster Interactions (ECI) multiplied by their respective multiplicity while the coefficient array a_i is the product of CVM coefficient times the probability degeneracy and the cluster multiplicity.
In case 2, we split the probability set into $p_{_B}$ for the $n_{_B}$ basic cluster probabilities and $p_{_S}$ for the sub-cluster ones ($n_{_B} + n_{_S} = n_p$ in case 1). We get :

$$\beta\, G = \sum_i^{n_{_B}} (\beta\, \widetilde{e}_i - \beta\, \mu\, \theta_i)\, p_{_B}(i) + \sum_j^{n_{_B}} a_j\, p_{_B}(j) \big(\ln p_{_B}(j) - 1 \big) + \sum_j^{n_{_S}} a_j\, p_{_S}(j) \, \big(\ln p_{_S}(j) - 1 \big) \tag{3}$$

$$p_{_S}(j) = \sum_i^{n_{_B}} \widetilde{M}\,(j,i)\; p_{_B}(i) \tag{4}$$

$$b(i) = \sum_i^{n_{_B}} J(k,i)\, p_{_B}(i) \quad \forall\, k \,\in\, [1, n_{_J}] \tag{5}$$

In the above expressions array $\widetilde{e_i}$ is the ECI phrased in terms of probabilities and array θ is the linear combination associated with point correlation. The variables $\mathbf{p_B}$ are box constrained and here involved in linear equalities rather than in Eq. 2 which defines a convex polyhedron.

In the building procedure of matrices, we generally generate redundant constraints that can be reduced by a Q.R decomposition with row pivoting, thus the Jacobian matrix J in Eq. 5 is a full rank matrix of rank $n_{_J}$. The components of the right hand side vector $b(i)$ are zero except for probability normalization where $b(i) = 1$ and optionally for given point correlation $b(i) = \xi_1$.
In both cases, taking advantage of sparsity and parallelism, most minimizations were carried out starting from the pure mean field solution, using the constrained Newton method [36] where $\beta\,\mu$ was treated as a simple Lagrange multiplier. From Hessian information, optimal solution derivative with respect to inverse temperature β or/and chemical potential were computed to speed-up computations for varying these parameters. Spinodal decomposition was determined by locating hessian zero eigenvalue either with respect to temperature at constant point correlation or the two boundary point correlations at given temperature. In the same way, miscibility gap was identified through the common tangent method, determining, by the Newton method, the two

point correlation functions $\xi_1^{\pm}$ with identical grand-potential and chemical potential. Numerical difficulties soon appeared owing to triangles ECI which shift spinodal or miscibility gap far away from stoichiometry. In such cases, when $\xi_1 \rightarrow \pm 1$, some probabilities become very small preventing convergence. In such case instead of using constrained Newton optimization, we used the NIM (Natural Iteration Method) [37] described for example in Ref.[34].

The slight difference of our algorithm and that of Pelizzola [34], is that Lagrange multipliers implied in the set of constraints of kind $J.X = 0$ were computed using either Broyden or Newton methods to solve a set of nonlinear equations rather than using a fixed point method. However, even NIM fails when $\mid \xi_1 \mid$ is too close from unity. In this limit, the solution is very close to a vertex of the polyhedron Eq.2, therefore some probabilities are nearly zero. While they practically do not contribute to the free energy, their contribution to derivatives is however dominant, so final successful attempts were conducted as follows.

By removing probabilities which correspond to highly excited states with respect to total occupancy of hydrogen atoms or vacancies, the number of variables from which minimizations were performed can be reduced in both formalisms. The method consists in reducing the dimensions of the problem, named "reduced probability" approach. Briefly stated, in case 1 for example, at a given iteration of the minimization process, let $n_{_p}$ the current number of probabilities and $n_{_c}$ the number of correlation functions. By n, we define the number of non redundant probabilities that fall below a given threshold ϵ, as example the machine precision, which can be safely removed. A row permutation of matrix $\mathbf{M}$ and related quantities such as the CVM coefficients is performed to bring these probabilities first. Then, a Q.R decomposition with column permutation of matrix $\mathbf{M}$ and related quantities allows to define a leading full rank submatrix, from which n probabilities and n correlation functions can be removed. The method applies also in case 2 under appropriate modifications and can be extended to ordered phases, or multi-component system.

The previously described method allows to sample at low temperature, however, it cannot reach 0 K, for which a ground state analysis was performed by minimizing, in

matrix form:

$$\mathbf{e}^T \mathbf{x} - \mu \xi_1 \text{ such } M \mathbf{x} \geq \mathbf{0} \tag{6}$$

$$(\widetilde{\mathbf{e}} - \mu\theta)^T \ \mathbf{p}_{\text{B}} \text{ such } \mathbf{b} = J \mathbf{p}_{\text{B}} \tag{7}$$

To solve the LP (linear programming) problem defined by Eq. 6, we used the interior point algorithm from Ref. [38] and to solve the LP problem defined by Eq. 7, we used the simplex based code LA04D adding upper bounds on probabilities [39]. In the case of PdH in addition to pure palladium $\xi_1 = -1$ and the hydride PdH $\xi_1 = +1$, we identified two other ground states occurring at $\xi_1 = -0.5$ that is a Pd_4H_3 structure and at $\xi_1 = -0.25$ or Pd_8H_5 through which low temperature phase diagram can be computed if required.

Finally to close this section, we notice that various algorithms to tackle minimization of the CVM free energy functional can be designed as for example projected gradient or reduced gradient methods [36]. It is also easy to build global optimizer that fulfils constraints such as differential evolution or genetic algorithm which rely on some random process. In this scope, we investigate MC for comparative purpose but also as a companion method. For example, solving the LP problem leads to a vertex from where in a next step a translationally invariant structure should be found. While spanning the whole range of chemical potential in LP is fast and highly reliable, the second task is easier in MC.

2.2. Monte Carlo simulations

Monte Carlo simulations which nowadays give "quasi exact" results, have been done within the grand canonical ensemble. The interstitial fcc sublattice is represented by a 4 by L^3 box with L the box length up to 20 to prevent size effect bias. An openMP code was written allowing 24 runs in parallel. In most cases, 20000 burns-in MC steps were disregarded and for 2^n ($n \geq 17$) MC sweeps, magnetization energy and correlations associated to ECI were recorded. Average and statistical errors of

magnetization, susceptibility, energy and specific heat were analyzed using binning and/or blocking methods [40].

We used MC methods, as a companion method to CVM, to locate the misciblility gap at given temperatures, using thermodynamical integration of the magnetization function of the chemical potential using Chebyshev polynomials, to supply data points where CVM may lack of accuracy. To this aim, we used:

$$G(\mu) = U(\mu_{-\infty}) + \mu - \int_{-\infty}^{\mu} \left(\xi_1(\tau) + 1\right) d\tau \quad (8)$$

$$G(\mu) = U(\mu_{+\infty}) - \mu - \int_{\mu}^{+\infty} \left(1 - \xi_1(\tau)\right) d\tau \quad (9)$$

$$G(\mu) = G(\mu_1) - \int_{\mu_1}^{\mu} \xi_1(\tau)\, d\tau \quad (10)$$

In equation 8 and 9, U refers to the internal energy of pure states (Pd and PdH) for which entropy is exactly zero and in equation 10 $G(\mu_1)$ refers to the grand potential of a reference state taken here as CVM output away from the phase separation. In all cases the CVM outputs match exactly the MC results within statistical error. The main advantage is to narrow the range of μ to be sampled in MC without loss of accuracy.

Simulated annealing and parallel tempering were also used to identify the crystal structures of previously predicted ground states by LP. The space group of the obtained crystal structures were identified via the phonopy code [41].
MC methods overcome many difficulties of CVM and graciously accommodate longer range interactions and more complex lattice structures without hard work. Such progress has been made in sampling techniques that even free energy or entropy can be computed, so this is obviously the right alternative to CVM for more complicated structures.

2.3. Structure Inversion Method

The ECI supplying both CVM and MC codes were determined using the Structure Inversion Method [35, 42] (SIM) within correlation function formalism based on DFT calculations. In our approach, only the energetic (enthalpic) contribution was used and not the temperature dependence that would allow the calculation of the phase diagram. In the CEM formalism, the energy of mixing is expanded in a complete and orthonormal basis in the configurational space $\{\phi\}_\alpha$:

$$E_{\mathrm{CEM}}^{\mathrm{mix}} = \sum_{\alpha} \nu_\alpha \xi_\alpha \tag{11}$$

with $\nu_\alpha = \langle E, \xi_\alpha \rangle$, the ECI, representing the contribution associated to the cluster α.

The Alloy Theoretic Automated Toolkit (ATAT) [43–45] was used to produce a relevant set of 25 long range ordered fcc super-structures for both Pd–H and Ni–H systems. In the frame of the SIM, the ECI were refined to fit an initial set of DFT calculated energies of mixing. The initial ECI are then used to predict the energy of a large number of super-structures. If a new ground-state super-structure is found, the corresponding DFT input data are generated and the calculation is done in order to add the new energy to the initial set. Otherwise the generated super-structure is judiciously selected in such a way that the variance component of the prediction error of a least-square fit is minimized.

The DFT calculations were carried out within the generalized gradient approximation (GGA) using the Perdew-Burke-Ernzerhof functional (PBE) [46, 47] with the Vienna Ab-initio Simulation Package (VASP) code [48, 49]. Calculations were performed with spin polarization for the Ni–H system. We used a high energy cutoff of 800 eV and a dense grid of k-points in the irreducible Brillouin zone ($\sim 2\pi \cdot 0.05$ Å), generated with the Monkhorst-Pack scheme [50]. For each compound, both the internal atomic coordinates and the lattice parameters were fully relaxed, so that the convergence of Hellmann- Feynman forces was better than 0.1 meV.Å^{-1}. The self-consistent total energy converged to less than 0.01 meV.

The energy of mixing at 0 K of a given super-structure $M\mathrm{H}_y$ with $0 \leq y \leq 1$ was calculated according to equation 12.

$$\Delta E_i^{\mathrm{mix}} = E_{M\mathrm{H_y}}^{\mathrm{tot}} - y \cdot E_{M\mathrm{H}}^{\mathrm{tot}} - (1-y) \cdot E_M^{\mathrm{tot}}. \tag{12}$$

3. Results

The DFT calculations of all the Ni–H super-structures resulted systematically in positive $\Delta E_i^{\mathrm{mix}}$ values. This reflects their instability with respect to the two-phase equilibrium between pure nickel and NiH and therefore explains the existence of a miscibility gap. Conversely, many ordered super-structures with negative energy of mixing were found in Pd–H system, in particular at high hydrogen compositions (Fig. 1). This includes the two previously reported super-structures $\mathrm{PdH}_{0.5}$ and $\mathrm{PdH}_{0.8}$ in $I4_1/amd$ and $I4/m$ space group respectively.

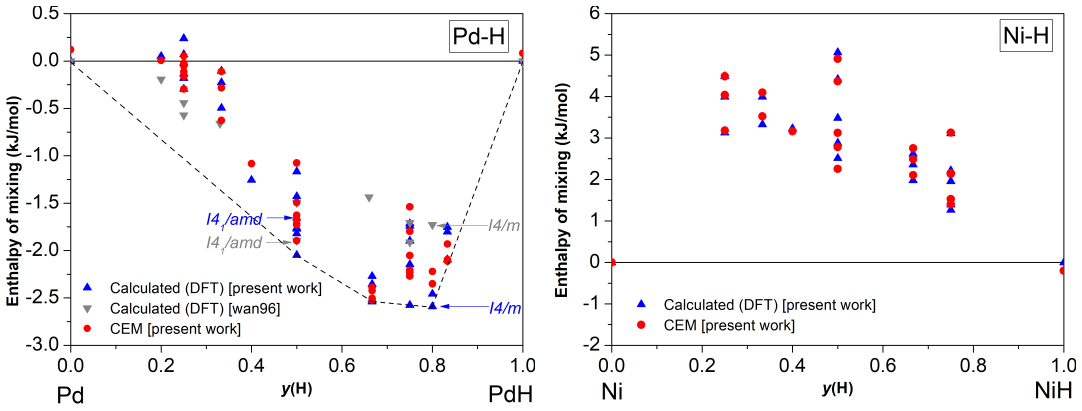

Figure 1. DFT calculated (blue) and CEM energies of mixing (red) of the ordered super-structures for Pd–H and Ni–H systems. Comparison with the DFT calculated values (gray) of Wang *et al.* [51].

On the basis of the DFT calculated energies of mixing, the ECI were refined within the ATAT code and the final set was selected on its predictive power quantified by the cross-validation (CV) score defined in Ref. [43] and constrained to confine within the 13-14 points. The chosen clusters are illustrated in Fig. 2 with the respective ECI sets listed in Table 2.

Using the listed ECI as input data for the CVM code, the thermodynamic quantities were calculated for Pd-H system (not for Ni-H which presents numerical instabilities

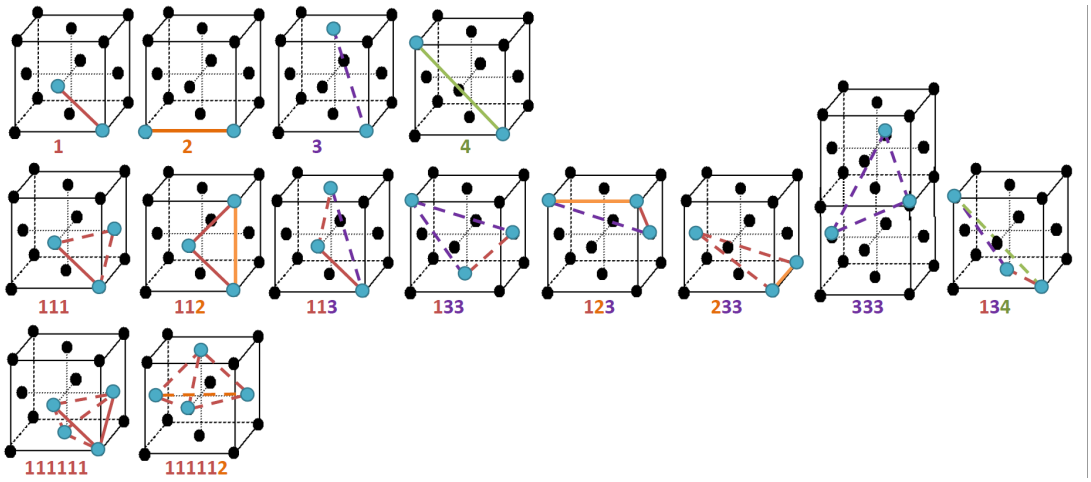

Figure 2. Chosen fcc cluster considered in the present work. from top to bottom: pairs, triplets and tetrahedra.

Table 2. ECI (eV) including multiplicity assessed on DFT calculations for Pd–H (CV=1.8 meV) and Ni–H (CV=1.6 meV). The pairs i are indexed in ascending order of atomic distance and are presented in Fig. 2.

cluster	multiplicity	pairs i	Pd–H	Ni–H
$\emptyset$	1	-	-0.016767	+0.033359
point	1	-	+0.027846	+0.015733
pair 1	6	1	+0.005922	-0.035916
pair 2	3	2	+0.004905	+0.005322
pair 3	12	3	+0.003216	-0.009924
pair 4	6	4	+0.003762	
triplet 1	8	1, 1, 1	-0.004240	-0.006520
triplet 2	12	1, 1, 2	-0.001800	-0.008172
triplet 3	24	1, 1, 3	-0.004968	
triplet 4	24	1, 3, 3	+0.005976	
triplet 5	24	1, 2, 3	-0.001680	
triplet 6	24	2, 3, 3	-0.005232	
triplet 7	8	3, 3, 3	-0.004536	
triplet 8	48	1, 3, 4	-0.011184	
tetraedron 1	2	1, 1, 1, 1, 1, 1		-0.000792
tetraedron 2	12	2, 1, 1, 1, 1, 1		+0.006912

within the spinodal domain) and is shown in Fig. 3 using canonical CVM calculations at 350 K. The point near the stoichiometric compositions could be obtained via the NIM and the minimization performed on reduced probability sets. CVM results within the spinodal should be considered with care as they do not correspond to true minimum. The resulting phase diagrams for both systems are represented on Fig. 4. One may note the excellent agreement between the CVM and MC for Ni–H system, validating the reliability of the results.

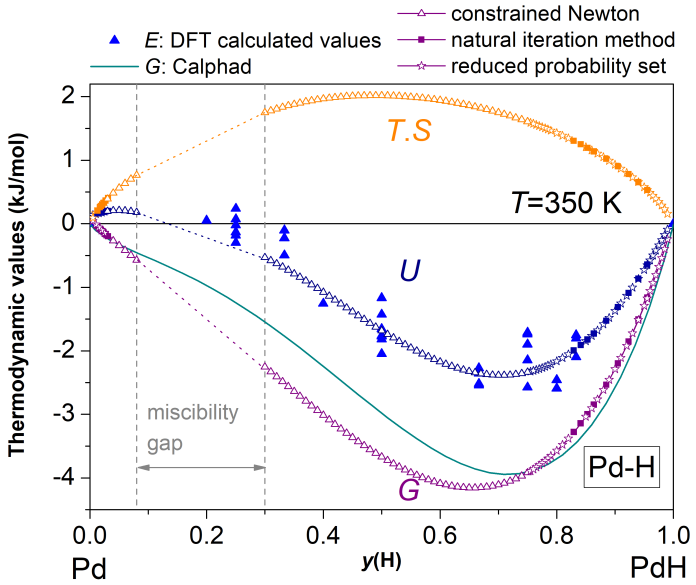

Figure 3. Thermodynamic quantities for Pd–H system obtained by CVM using 3 different minimization algorithms. Comparison with the Calphad model [29].

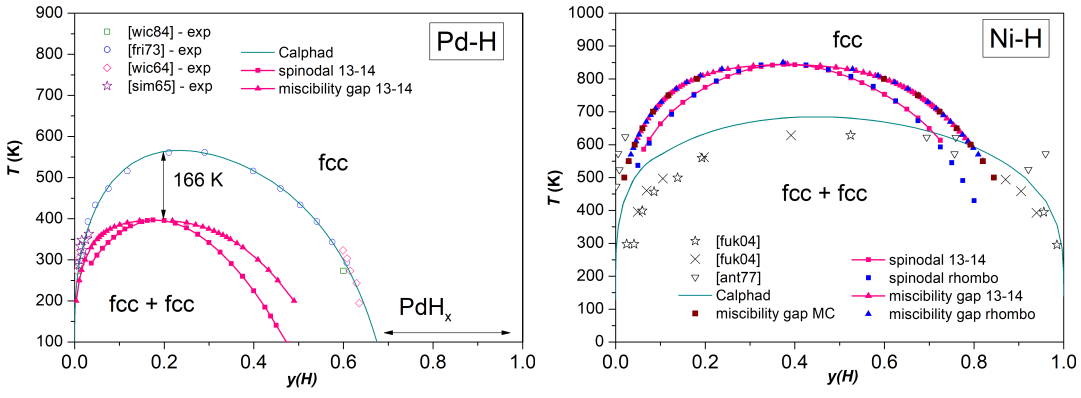

Figure 4. Phase diagrams and spinodals of Pd–H and Ni–H systems obtained by CVM. Comparison with the Calphad models [29, 32] and experimental data.

Two new ordered super-structures $PdH_{0.625}$ and $PdH_{0.75}$ (details on Tab. 3) were identified on the ground-state by using MC on the ECI set generated by CEM.

Table 3. Monte Carlo predicted ground-state for Pd–H system suing the ECI set of Table 2: Composition, Space Group (S.G.) (number), Wyckoff positions.

H/Pd	S.G. (number)	Wyckoff positions	
0.625	$Im\bar{3}m$ (229)	Pd: 2*a*, 6*b*, 24*h*	H : 8*c*, 12*e*
0.75	$I4_132$ (214)	Pd: 8*a*, 24*h*	H : 24*g*

4. Discussion

One may note that the ordering observed for the Pd–H system is almost unique among *M*–H systems and was only observed on the O-sites of rare-earth hydrides RH_{2+x} in which hydrogen occupies all the tetrahedral sites of the fcc lattice [52].

The two experimentally observed intermediate compounds $PdH_{0.5}$ and $PdH_{0.8}$ have been calculated by DFT and one of them ($I4_1/amd$) is actually found on the ground state. However, the present DFT calculations on CEM superstructures pointed out that several other PdH_x compounds are also stable at 0 K (Fig. 1). The precision of the DFT calculation is indeed too limited to compare the super-structure relative stabilities within a so close energy range and to determine a reliable groundstate. Indeed, previous DFT calculations [51] lead to a different groundstate with an average difference of about 3.6×10^{-3} eV with the present calculations. Besides, the vibrational contribution to the energy of mixing may also be non negligible, as shown in previous work [53]. In this frame, the predictions of CVM and MC inevitably differ slightly from the observed ordered configurations. In fact, the two new structures of Table 3 predicted by CVM and MC and recalculated by DFT are not exactly found on the DFT ground state but the associated energy calculated by CEM with the same set of ECI place them on the ground state.

At first sight, Pd–H and Ni–H systems seem to be very similar. Palladium and nickel both adopt the fcc structure and have the same valence electronic structure, suggesting similar chemical bonds with hydrogen. Second, in presence of hydrogen, both metals appear to have similar behaviors. Indeed, hydrogen atoms settle on the same O-sites

and the structure of the hydride has the NaCl structure type in both case. Besides, the α/α' phase separation is observed in both cases and the resulting miscibility gap closes at similar temperatures.

A first difference came from the stability of the formed hydrides: while palladium hydride can be formed easily at pressures of around 10 mbar at room temperature, a couple of kilobars is necessary to form Ni hydride. This can be fairly well explained by the larger cell volume of Pd compared to Ni host structure and by the DFT calculation of the very different enthalpies of formation of Pd and Ni hydrides as shown in our recent work [9].

Even more surprising, in the frame of the present study is the opposite sign of the energy of mixing (Fig.1). This difference can be interpreted by analyzing the calculated density of state (DOS) of the ordered super-structures. DOS of pure metal and stoichiometric hydrides are given in supplementary materials. A simple picture is given in Fig. 5, showing the evolution of DOS at the Fermi level, DOS(E_F), as a function of y(H) for both Pd–H and Ni–H systems.

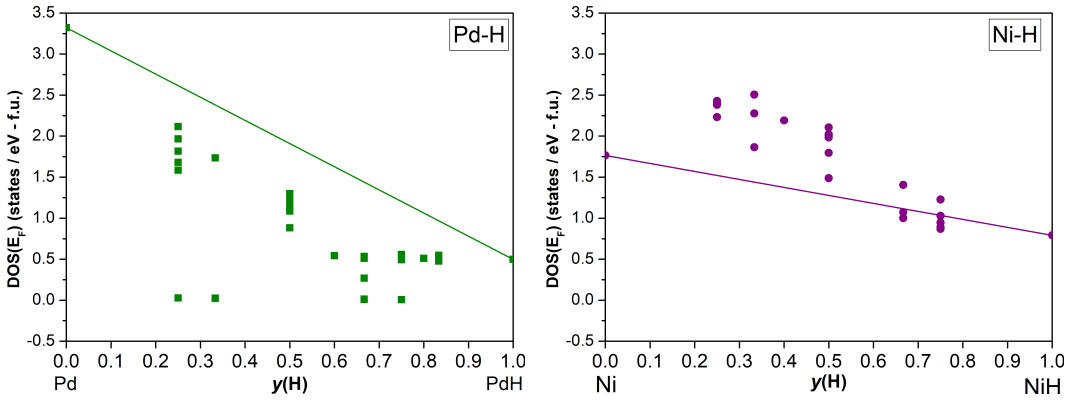

Figure 5. DOS at the Fermi level as a function of y(H) for both Pd–H and Ni–H systems.

In comparison with Pd metal, Ni presents more localized $d-$bands structure and, without spin polarisation, the DOS at Fermi level is higher for Ni (4.5 states by eV). As a consequence, to reduce its DOS(E_{F}) to 1.8 (Stoner criterion), a ferromagnetic state is found more stable for Ni and the majority spin bands are almost filled. The electronic structure is affected by hydrogen absorption. In Ni–H system, electrons given by H lead to a progressive filling of the 3d-Ni bands and to an increase of

the DOS(E_F) up to a maximum at $y = 0.33$ (corresponding to the filling of a peak in minority spin), before a decrease of DOS(E_F) with y. This is detrimental to the formation of intermediate compounds. On the contrary for PdH_y compounds, the DOS(E_F) decreases as a function of hydrogen concentration y, with respect to its values for Pd and PdH. As a consequence, the energy of mixing for Pd–H system is negative which explains the presence of stable ordered super-structures.

Regarding the Ni–H system, the positive sign of the energy of mixing is reflected in the ECI associated to the first neighbour pair, which has a strongly negative value, thus favouring like-pairs. It accounts for the tendency of hydrogen atoms to be surrounded by other hydrogen atoms yielding the formation of a miscibility gap. Contrarily, for the Pd–H system, the positive first neighbour pair ECI leads to the ordering tendency. The sign is the same as in the models of Bond and Ross [24] and Mohri and Oates [26, 27]. Interestingly, the ECI associated to the second pair in Pd–H was found dominant against that of the first pair. A similar result was found by Demangeat *et al.* [54] within a tight-binding model, obtaining also positive values for the first ECI, the second being about twice the first. Besides, the triplet interactions introduce an asymmetry in the phase diagrams particularly pronounced in Pd–H system, favouring the solid solution stability on the higher composition range and the phase separation on the lower composition range.

Figure 4 shows the predicted miscibility gap boundary for Pd–H and Ni–H, compared with experimental determination. The data resulting from CVM and MC were voluntary shifted to be distinguished. These two statistical methods though radically different since the CVM relies on a variational principle while MC rest on Markov process, lead to the same outcome for magnetization. It should be quoted that this agreement remains true for the magnetic susceptibility calculated analytically by derivation in CVM and from fluctuations in MC. These results were expected since the 13-14 points cluster is already accurate in the Ising model and as a general trend mean field theory improves significantly with the number of ECI, as well as the number of chemical compounds. In Ni–H, the phase separation is driven by the positive sign of

the energy of mixing on the complete composition range (Fig. 3). The critical point is slightly shifted to the left by the triplet contribution.

Very differently, in Pd–H system, the miscibility gap arises from two curvature changes of the negative free energy of mixing (Fig. 3). It explains very well the simultaneous presence of a miscibility gap and negative enthalpies of mixing correlated with the observation of super-structures, very unlikely at a first glance. Compared with the experimental data, the critical point of Pd–H is underestimated by 166 K while the one of Ni–H is overestimated by 158 K (Fig. 4). The discrepancy reflects the lack of precision of the raw ECI data, which are volume independent in our model. But it may also arise from macroscopic effect like coherency strain between the α and α' phase boundary as suggested by Alefeld [22, 23] which favours the phase separation. Other mechanisms as potential mechanical instability also require further investigation. However, considering that only theoretical input were used, the predictions are remarkable. The present results show that the only configurational contribution to the thermodynamic quantities is sufficient to describe the behavior of both systems and to induce both the miscibility gap and the ordering phenomena for Pd–H, without the need of either long-range elastic interaction [24] or lattice expansion contribution [26, 27].

5. Conclusion

Both CVM and MC simulations based on DFT calculations allowed to obtain comprehensive descriptions of both Pd–H and Ni–H systems. We would like to underline the complementarity of the two techniques, allowing to validate the results given by the same inputs. MC simulation allows to identify the atom positions of the ground-state and the CVM improves the MC calculation time providing integration constants. Our model could be improved by taking into account the effect of lattice vibration and distortion [55] in order to improve the accuracy on the DFT calculated energies. The effects of the important volume expansion on the atomic interactions could also be considered. However, both MC and CVM techniques allowed to show that miscibility gaps in Pd–H and Ni–H systems originate from very different physical quantities: a change of the curvature of the negative free energy for Pd–H and a positive energy

of mixing in the case of Ni–H. For Pd–H system, the simultaneous presence of low temperature ordering and a miscibility has been shown to be compatible. Compared to the previous phenomenological models [24, 26, 27], the energy and entropy contribution to the Gibbs energy could be determined from physical inputs only without the use of any empirical parameter.

Acknowledgements

This work has benefited from a French government grant managed by ANR within the framework of the national program Investments for the Future ANR-11-LABX-022-01. DFT calculations were performed using HPC resources from GENCI-CINES (Grant 2018-96175). We thank Pr Tetsuo Mohri from IMR, Tohoku University who provided insight that greatly assisted the research. Ying Chen and Arkapol Saengdeejing are also acknowledged to have initiated the CEM work.

References

[1] L. Schlapbach, Technology: Hydrogen-fuelled vehicles, Nature 460 (2009), pp. 809–811.

[2] B.D. Adams and A. Chen, The role of palladium in a hydrogen economy, Mater. Today 14 (2011), pp. 282–289.

[3] R.K. Joshi, S. Krishnan, M. Yoshimura, and A. Kumar, Pd nanoparticles and thin films for room temperature hydrogen sensor, Nanoscale Res. Lett. 4 (2009), pp. 1191–1196.

[4] G. Sandrock and R.C. Bowman, Gas-based hydride applications: recent progress and future needs, Journal of Alloys and Compounds 356-357 (2003), pp. 794 – 799, proceedings of the Eighth International Symposium on Metal-Hydrogen Systems, Fundamentals and Applications (MH2002).

[5] F. Cuevas, J.M. Joubert, M. Latroche, and A. Percheron-Guégan, Intermetallic compounds as negative electrodes of ni/mh batteries, Applied Physics A 72 (2001), pp. 225–238.

[6] J.M. Joubert, M. Latroche, and A. Percheron-Guégan, Metallic hydrides ii: Materials for electrochemical storage, MRS Bull. 27 (2002), pp. 694–698.

[7] J. Worsham, M. Wilkinson, and C. Shull, Neutron-diffraction observations on the

palladium-hydrogen and palladium-deuterium systems, J. Phys. Chem. Solids 3 (1957), pp. 303–310.

[8] Wollan, E. O., Cable, J. W., Koehler, W. C., The hydrogen atom positions in face centered cubic nickel hydride, J. Phys. Chem. Solids 24 (1963), pp. 1141–1143.

[9] N. Bourgeois, J.C. Crivello, P. Cenedese, and J.M. Joubert, Systematic first-principles study of binary metal hydrides, ACS Combinatorial Science 19 (2017), pp. 513–523.

[10] O. Blaschko, P. Fratzl, and R. Klemencic, Model for the structural changes occurring at low temperatures in PdD_x, Phys. Rev. B 24 (1981), pp. 277–282.

[11] O. Blaschko, Structural features occurring in PdD_x within the 50 K anomaly region, J. Less-Common Met. 100 (1984), pp. 307–320.

[12] I. Anderson, D. Ross, and C. Carlile, The structure of the γ phase of palladium deuteride, Phys. Lett. A 68 (1978), pp. 249–251.

[13] I.S. Anderson, D.K. Ross, and C.J. Carlile, The 50 K transition in β-phase palladium deuteride observed by neutron scattering, J. Phys. C: Solid State Phys. 11 (1978), pp. L381—L384.

[14] T.E. Ellis, C.B. Satterthwaite, M.H. Mueller, and T.O. Brun, Evidence for H (D) ordering in PdH_x (PdD_x), Phys. Rev. Lett. 42 (1979), pp. 456–458.

[15] D. Ross, M. McKergow, D. Witchell, and J. Kjems, Neutron diffraction studies of domain growth associated with the 50 K anomaly in Pd–D, J. Less-Common Met. 172 (1991), pp. 169–182.

[16] E. Wu, S.J. Kennedy, E.M.A. Gray, and E.H. Kisi, The ordered structure of $PdD_{0.78}$ at 70 - 75 k, J. Phys.: Condens. Matter 8 (1996), pp. 2807–2813.

[17] J.R. Lacher and R.H. Fowler, The statistics of the hydrogen-palladium system, Math. Proc. Cambridge Philos. Soc. 33 (1937), pp. 518–523.

[18] A. Harasima, T. Tanaka, and K. Sakaoku, Cooperative phenomena in Pd-H system I, J. Phys. Soc. Jpn. 3 (1948), pp. 208–213.

[19] H. Brodowsky, Das system palladium/wasserstoff, Z. Phys. Chem. 44 (1965), pp. 129–142.

[20] W. Oates, Thermodynamic properties of the Pd–H system, J. Less-Common Met. 88 (1982), pp. 411–424.

[21] J.W. Cahn, On spinodal decomposition, Acta Metall. 9 (1961), pp. 795–801.

[22] G. Alefeld, Wasserstoff in metallen als beispiel für ein gittergas mit phasenumwandlungen, Phys. Status Solidi 32 (1969), pp. 67–80.

[23] G. Alefeld, Phase transitions of hydrogen in metals due to elastic interaction, Ber. Bun-

senges. Phys. Chem. 76 (1972), pp. 746–755.

[24] R.A. Bond and D.K. Ross, The use of monte carlo simulations in the study of a real lattice gas and its application to the α' Pd-D system, J. Phys. F Met. Phys. 12 (1982), pp. 597–609.

[25] D. Picton, R. Bond, B. Bowerman, D. Ross, D. Witchell, I. Anderson, and C. Carlile, The influence of H–H interactions on the phase diagram of Pd–H, J. Less-Common Met. 88 (1982), pp. 133–140.

[26] T. Mohri and W.A. Oates, CVM–based calculation of the Pd–H phase diagram in the high temperature region, Mater. Trans. 43 (2002), pp. 2656–2661.

[27] T. Mohri and W.A. Oates, Theoretical investigation of Pd–H phase equilibria by the cluster variation method, J. Alloy. Compd. 330-332 (2002), pp. 14–19.

[28] D.E. Nanu and A.J. Böttger, Phase stabilities of Pd-based alloys for membranes for hydrogen gas separation: A statistical thermodynamics approach, J. Alloy. Compd. 446-447 (2007), pp. 571–574.

[29] J.M. Joubert and S. Thiébaut, A thermodynamic description of the system Pd-Rh-H-D-T, Acta Mater. 59 (2011), pp. 1680–1691.

[30] J. Ågren, Y. Brechet, C. Hutchinson, J. Philibert, and G. Purdy, Thermodynamics and Phase Transformations: the Selected Works of Mats Hillert, EDP Sciences, Les Ulis Cedex A, 2006.

[31] H.L. Lukas, S.G. Fries, and B. Sundman, Computational Thermodynamics: the Calphad Method, Vol. 131, Cambridge University Press, Cambridge, 2007.

[32] N. Bourgeois, J.C. Crivello, A. Saengdeejing, Y. Chen, P. Cenedese, and J.M. Joubert, Thermodynamic modeling of the Ni–H system, J. Phys. Chem. C 119 (2015), pp. 24546–24557.

[33] R. Kikuchi, A theory of cooperative phenomena, Phys. Rev. 81 (1951), pp. 988–1003.

[34] A. Pelizzola, On three new cluster variation approximations, Physica A 211 (1994), pp. 107–123.

[35] J. Sanchez, F. Ducastelle, and D. Gratias, Generalized cluster description of multicomponent systems, Phys. A 128 (1984), pp. 334–350.

[36] M. Minoux, Programmation mathématique. Théorie et algorithmes, Dunod, 1983.

[37] R. Kikuchi, Superposition approximation and natural iteration calculation in cluster - variation method, The Journal of Chemical Physics 60 (1974), pp. 1071–1080.

[38] N.I.M. Gould, D. Orban, and P.L. Toint, Galahad, a library of thread-safe fortran 90

packages for large-scale nonlinear optimization, ACM Trans. Math. Softw. 29 (2003), pp. 353–372.

[39] HSL, A collection of fortran codes for large scale scientific computation, A collection of Fortran codes for large scale scientific computation, http:/www.hsl.rl.ac.uk (2013).

[40] H. Flyvbjerg and H.G. Petersen, Error estimates on averages of correlated data, J. Chem. Phys. 91 (1989), pp. 461–466.

[41] A. Togo and I. Tanaka, First principles phonon calculations in materials science, Scr. Mater. 108 (2015), pp. 1–5.

[42] J.W.D. Connolly and A.R. Williams, Density-functional theory applied to phase transformations in transition-metal alloys, Phys. Rev. B 27 (1983), pp. 5169–5172.

[43] A. van de Walle, M. Asta, and G. Ceder, The Alloy Theoretic Automated Toolkit: A user guide, Calphad 26 (2002), pp. 539–553.

[44] A. van de Walle, Multicomponent multisublattice alloys, nonconfigurational entropy and other additions to the Alloy Theoretic Automated Toolkit, Calphad 33 (2009), pp. 266–278.

[45] A. van de Walle and G. Ceder, Automating first-principles phase diagram calculations, J. Phase Equilib. 23 (2002), pp. 348–359.

[46] J.P. Perdew, M. Ernzerhof, and K. Burke, Rationale for mixing exact exchange with density functional approximations, J. Chem. Phys. 105 (1996), pp. 9982–9985.

[47] J.P. Perdew, K. Burke, and M. Ernzerhof, Generalized gradient approximation made simple, Phys. Rev. Lett. 78 (1997), pp. 1396–3868.

[48] G. Kresse and J. Furthmüller, Efficient iterative schemes for ab initio total-energy calculations using a plane-wave basis set, Phys. Rev. B 54 (1996), pp. 11169–11186.

[49] G. Kresse and D. Joubert, From ultrasoft pseudopotentials to the projector augmented-wave method, Phys. Rev. B 59 (1999), pp. 1758–1775.

[50] H.J. Monkhorst and J.D. Pack, Special points for brillouin-zone integrations, Phys. Rev. B 13 (1976), pp. 5188–5192.

[51] Y. Wang, S.N. Sun, and M.Y. Chou, Total-energy study of hydrogen ordering in PdH_x ($0 \leq x \leq 1$), Phys. Rev. B 53 (1996), pp. 1–4.

[52] P. Vajda, Hydrogen in rare-earth metals, including $RH2 + x$ phases, in Handb. Phys. Chem. Rare Earths, Vol. 20, Elsevier, Amsterdam, 1995, pp. 207–291.

[53] N. Bourgeois, J.C. Crivello, P. Cenedese, P.B. V., and J.M. Joubert, Vibration analysis of interstitial hydrogen, deuterium and tritium in metals: consequences on the isotope

effect, submitted in Journal of Physics: Condensed Matter (2018).

[54] C. Demangeat and M. Khan, Chemical binding energies of point defects in palladium doped with hydrogen and d impurities, J. Phys. 41 (1980), pp. 1001–1007.

[55] Y. Yamada and T. Mohri, Lattice statistics and dynamics within cluster variation method, Mater. Trans. 57 (2016), pp. 481–487.